Hindawi Publishing Corporation
Modelling and Simulation in Engineering
Volume 2011, Article ID 754257, 8 pages
doi:10.1155/2011/754257

Research Article

Gear Defect Modeling of a Multiple-Stage Gear Train

Andrew Sommer, Jim Meagher, and Xi Wu

Department of Mechanical Engineering, California Polytechnic State University, San Luis Obispo, CA 93407-0358, USA

Correspondence should be addressed to Xi Wu, xwu@calpoly.edu

Received 31 March 2011; Accepted 10 June 2011

Academic Editor: Xiaosheng Gao

Copyright © 2011 Andrew Sommer et al. This is an open access article distributed under the Creative Commons Attribution License, which permits unrestricted use, distribution, and reproduction in any medium, provided the original work is properly cited.

This study demonstrates the transient and steady state dynamic loading on teeth within a two-stage gear transmission arising from backlash and geometric manufacturing errors by utilizing a nonlinear multibody dynamics software model. Backlash between gear teeth which is essential to provide better lubrication on tooth surfaces and to eliminate interference is included as a defect and a necessary part of transmission design. Torsional vibration is shown to cause teeth separation and double-sided impacts in unloaded and lightly loaded gearing drives. Vibration and impact force distinctions between backlash and combinations of transmission errors are demonstrated under different initial velocities and load conditions. The backlash and manufacturing errors in the first stage of the gear train are distinct from those of the second stage. By analyzing the signal at a location between the two stages, the mutually affected impact forces are observed from different gear pairs, a phenomenon not observed from single pair of gears. Frequency analysis shows the appearance of side band modulations as well as harmonics of the gear mesh frequency. A joint time-frequency response analysis during startup illustrates the manner in which contact forces increase during acceleration.

1. Introduction

Gear trains with different designs play very important roles in automobiles, helicopters, wind turbines, and other modern industries. Excessive loading on the gear teeth may arise due to the combination of gear backlash and teeth defects. Without vibration health monitoring to ensure proper operation performance will degrade.

Dubowsky and Freudenstein [1, 2] developed a theoretical model to investigate the dynamic response of a mechanical system with clearance. Based on this research, Azar and Crossley [3] explored the dynamic behaviors of the engaged gearing systems with gear backlash, time-varying stiffness, and damping of the gear teeth. Compared with above investigations, Yang and Sun [4] developed a more realistic dynamic model for a spur gear system with backlash. By taking the involute tooth profile into consideration, they were able to account for material compliance, energy dissipation, time-varying mesh stiffness, and damping due to the contact teeth-pair alternating between one and two during the gear engagement. In order to accurately simulate the gear dynamic behavior, the gear mesh stiffness between meshing gear pairs should include at least two factors: local Hertzian deformation and tooth bending. Even though the authors only considered the Hertzian contact stiffness, the dynamic simulations for free vibration, constant load operation, and sinusoidal excitation presented insightful results.

Two notable review papers that discuss the numerical modeling of gear dynamics are by Özgüven and Houser in 1988 [5] and by Parey and Tandon in 2003 [6]. Özgüven and Houser categorized the models as dynamic factor models, models with tooth compliance, models for gear dynamics, those for rotor dynamics, and those for torsional vibration. The listed goals for the studies included reliability, life, stress, loading, noise, and vibratory motion. Curiously, condition monitoring was not included. Early work modeled the meshing stiffness as either an average or piecewise linear variation. Parey and Tandon's review concentrated mostly on the modeling of defects but includes an extensive compilation of various lumped parameter models. Dalpiaz et al. [7] investigated a gear pair with a fatigue crack and discussed the effectiveness and sensitivity of the time-synchronous average (TSA) analysis, cyclostationary analysis, and traditional cepstrum analysis on the basis of experiment. Parey et al. [8] developed a six DOF nonlinear model for a pair of spur

gears on two shafts, calculated the Hertzian stiffness for the tooth surface contact, and implemented the empirical mode decomposition (EMD) method to simulate the different defect widths. Many authors [9–12] utilized different methods of estimating time-varying stiffness in order to get practical dynamic simulation results. Meagher et al. [13] presented three different dynamic system modeling strategies currently being used by researchers to identify diagnostic indicators of gear health: a strength of materials-based lumped parameter model, nonlinear quasistatic finite element modeling, and rigid multibody kinematic modeling with nonlinear contact stiffness. This research contrasts these methods of modeling gear dynamics by comparing their predicted stiffness cycle and its effect on dynamic response. Data from experiments are shown for the high contact ratio pair.

Previous research shows that the signal patterns due to the combination of backlash, time-varying gear mesh stiffness, and the involute profile errors are very complicated and highly depend on gear train design and configurations. In other words, the signals from a specific gearing system are difficult to interpret until a series of modeling, testing, and data processing work are carried out. However, it is not realistic to experimentally test each type of gear train for the specific fault patterns. To solve this issue, a virtual experiment method based on multibody dynamics and nonlinear contact mechanics simulation is presented. Ebrahimi and Eberhard [9] used multibody dynamics software to model gear mesh stiffness using a rigid-elastic model. Hertzian contact at the gear interface is used to represent gear elasticity as a compromise over fully elastic models, thereby reducing computational effort. Kong et al. [14] modeled a large industrial gearbox used in a 12 m^3 electric mining shovel. The nonlinear contact mechanics is analyzed to predict the bearing support force variation and gear tooth loading of ideal gears and gears with defects using multibody dynamics software. No gear backlash was considered. In this study, the authors demonstrate the importance of accurate geometric modeling of gear tooth involutes, and realistic center distance separation on the transient response of ideal and defective gears. The highly nonlinear character of loading and geometry requires special attention to Hertzian contact modeling. Once modeled accurately, double-sided tooth impacts and associated loading can be determined as well as superposition of effects at a shaft intermediate to sets of gears. The analysis from frequency domain indicates that an eccentric tooth on a gear installed on the intermediate shaft results in a significant increase in force magnitude components. The amplitude of the spectral line at the first-stage gear mesh frequency increases dramatically.

2. Multibody Kinematic Model of Slider-Crank Mechanism with Two-Stage Gear Train

In order to investigate how the interaction of backlash and manufacturing errors affects the dynamic behavior and contact forces of a multiple stage gearing system, the slider-crank mechanism shown in Figure 1 is studied. The gear

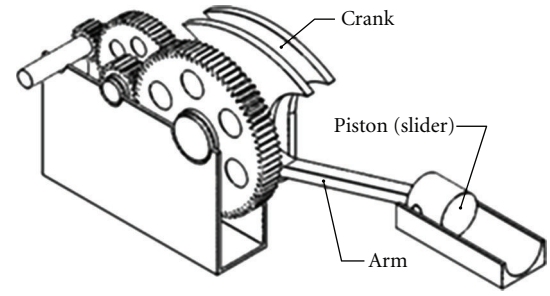

Figure 1: Crank-slider mechanism.

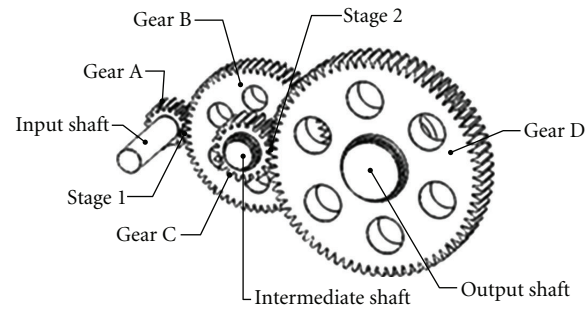

Figure 2: Two-stage gear train.

Table 1: Gear design parameters.

Modules (mm/tooth)	$m_1 = 4$; $m_2 = 5$
Number of teeth	$Z_a = 17$; $Z_b = 60$; $Z_c = 19$; $Z_d = 72$
Standard pitch circle diameter (mm)	$D_a = 68$; $D_b = 240$; $D_c = 95$; $D_d = 360$
Total gear ratio	13.375
Pressure angle	20°

bodies shown in Figure 2 are rigid, but the contact surfaces are modeled using a penalty-based nonlinear contact formulation. The contact force, $F = K(d)^e - cv$, is composed of an elastic and damping portion [15]; d is the penetration depth. The damping force, cv, is proportional to impact velocity, v. The stiffness coefficient, K, is taken to be the average value of stiffness over one tooth mesh cycle. The force exponent, e, was determined from trial simulations. The damping coefficient generally takes a numeric value between 0.1% and 1% of K. The determination of force exponents however is not obvious and must be based on experience. The gear design parameters and simulation parameters are shown in Tables 1 and 2, respectively.

The MSC.ADAMS IMPACT algorithm was chosen as the contact force model because of its robustness in numerical integration. The restitution model is extremely sensitive to the duration of the contact event and is best suited for impulse type simulations. It is not ideal for time histories that include a large number of contact events in which the force vector is not known beforehand. The stiffness parameter is reasonable for this lightly loaded steel gear

Table 2: Simulation parameters.

Backlashes (mm)	$B_1 = 0.05$; $B_2 = 0.08$
Material properties	$E = 2.07 \times 10^{11}$ Pa; $\nu = 0.29$; $\rho = 7801\,\text{kg/m}^3$
Force exponent	2.2
Penetration	10^{-7} mm
Stiffness	2×10^7 N/mm

pair and was determined via a trial and error method. The response of interest occurs over a very short time interval, around one hundred milliseconds. Because the damping force in meshing gears is such a small percentage of K, its affect on the simulation results is not significant. Therefore, the damping coefficient is kept as near to zero as possible to simplify the numerical solver routine. Penetration depth is defined here as the depth at which the damping forces become active. Similarly, modification of this value does not have a significant effect on response of either gear. An eccentric tooth on Gear A is generated by linearly translating the involute profile 0.0045 mm from the perfect geometric position; the chipped tooth is created by removing the mass of a single tooth, shown in Figure 3.

3. Transient Response after Power Loss

The "perfect" waveform represented in Figure 4 is the response of all four gears with perfect geometry and prescribed backlash. The "chipped" curve is the response of an input pinion with a chipped tooth; all other gears are perfect. The coordinate orientation is such that a force *from the pinion to the gear* is considered positive. This simulation models the machine operating at steady-state conditions and suddenly losing power. The system is given an initial velocity on each shaft that corresponds to its rotary speed under operating conditions. From the top two plots of Figure 4, the initial position of the gears is such that neither stage is in contact at the beginning of the simulation. The assumption is that with loss of power there will be separation of teeth due to load removal and inertia effects so that the simulation begins at this condition. Therefore, all three shafts are rotating without any impacts until Gear C touches Gear D at approximately 12 ms. Gear B touches Gear A around 15 ms, causing the contacts in Stage 1 to increase in frequency for the next 20 ms.

The response of the intermediate shaft is due to a superposition of the impacts in Stage 1 and Stage 2. The angular velocity of the intermediate shaft is shown to be combination of the other two shafts' angular velocities. Double-sided impacts are evident in the time history of the Y-component of force in Stage 1. When the sign on the force alternates at a similar magnitude, it indicates impacts of the same tooth in alternate directions.

For the chipped pinion case, the impact force occurs at an earlier time. This can be explained in part through the reduction in inertia. The mass moment of interia of

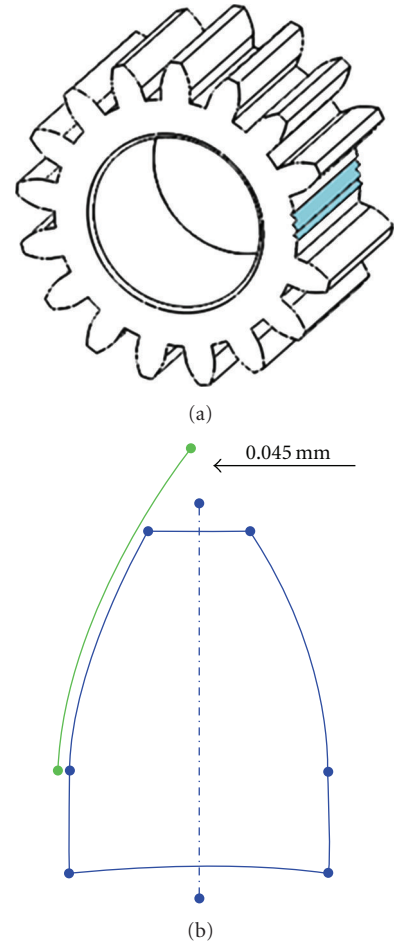

Figure 3: Geometric defects including (a) chipped tooth of Gear A and (b) eccentric tooth of Gear C.

the perfect input pinion is $I_{zz} = 1.06e-3\,\text{kg-m}^2$, while the chipped tooth pinion is $I_{zz} = 1.04e-3\,\text{kg-m}^2$. This is a reduction of 1.76%. The chipped pinion will experience a larger acceleration for a given impact force. The teeth neighboring the chipped tooth will contact the mating gear sooner than it would with the standard inertia.

The force response in Stage 2 is depicted in Figure 5. The first and second contacts occur at nearly the same time for both the perfect and chipped cases. With perfect mesh geometry, Gear D experiences three single-sided impacts for $10 \le t \le 30$ ms. With a chipped pinion tooth, Gear D only experiences two single-sided impacts during the same interval.

An impact occurs in Stage 2 before Stage 1; at first this may seem counterintuitive. The initial velocities given to each shaft are based upon their rated operating speed. The bearings are modeled as frictionless, constraining all degrees of freedom except for rotation in the normal plane. The relative velocity on the pitch circle of Gear C and Gear D is slightly larger than between Gear A and Gear B. For initial conditions in which the relative velocity between Gear A and Gear B is larger than between Gear C and Gear D, the opposite would occur.

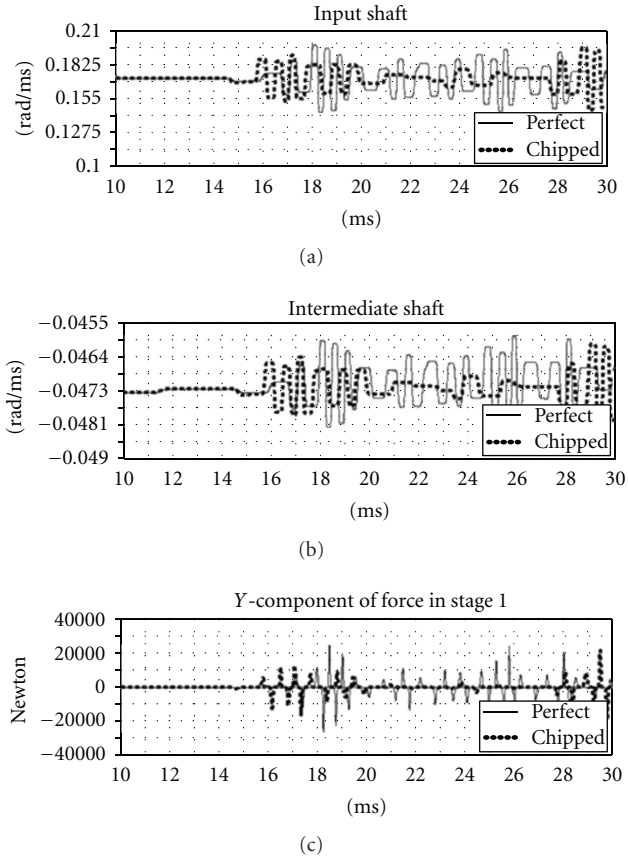

Figure 4: Free vibration response with input shaft, 167.5 rad/s; intermediate shaft, −73.5 rad/s; output shaft, 12.5 rad/s.

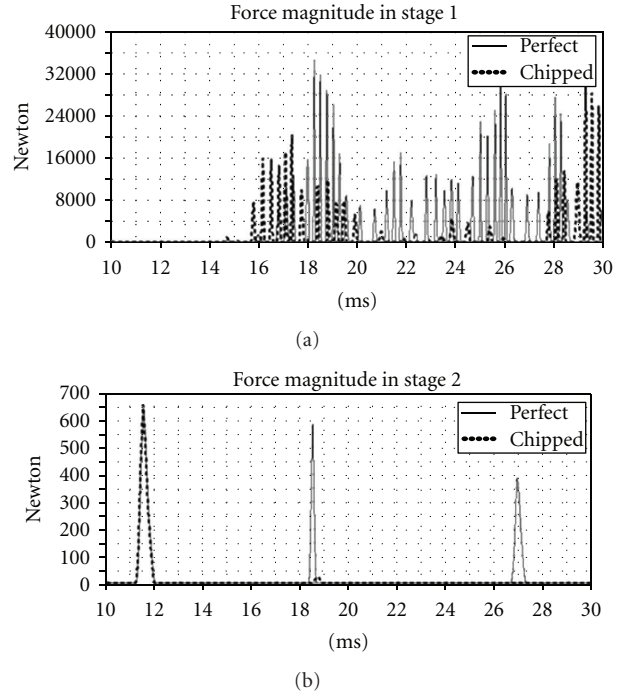

Figure 5: Comparison of the force magnitudes of Stage 1 and Stage 2 with initial conditions: input shaft, 167.5 rad/s; intermediate shaft, −73.5 rad/s; output shaft, 12.5 rad/s.

The system is modeled as the interaction of three rigid bodies. The first is the input shaft and Gear A. The second is Gear B, the intermediate shaft, and Gear C. The third is Gear D, the output shaft, and the crank. The third body has an inertial mass at least one order of magnitude larger than the other two bodies. Its velocity changes more slowly than for the other two bodies due to inertia effects. The small delay between responses around 18.5 ms can be attributed to the chipped tooth. Because the tooth is chipped, the force response in Stage 2 is slightly delayed.

Figure 6 shows the relative displacement between Gear C and Gear D in Stage 2. Any point on this plot defines the relative position of Gear C and Gear D for any give time. The contacts in the first stage create high frequency oscillations in the angular position of Gear C. The large-scale motion of Gear C is due to the contacts in the second stage, and Gear C moves between the teeth of Gear D. The quantity $S = R_g\theta_g - R_p\theta_p$ for the second stage appears as a jagged line. These small peaks correspond directly to the force changes in Stage 1, shown in Figure 4. Once Gear C makes contact with Gear D, the response becomes smoother. The effect is still there, but the speed of Gear D is now changing more rapidly and these smaller position changes are more difficult to distinguish.

For the case with a chipped tooth on the input pinion, the entire curve is shifted forward in time. Although the impacts in Stage 1 occur earlier, the overall effect in Stage 2 is delayed. The chipped tooth causes Stage 1 to become more excited, as a result it takes longer for the contact in Stage 2 to occur.

4. Start-Up Simulation

A practical step torque of the form $T(1 - e^{t/\tau})$ is applied to the input shaft with amplitude of 149.123 N-m at 100 ms to simulate a start-up accelerating condition.

From Figure 7, the gears in each mesh come to an equilibrium position in which they remain in contact. This must be true for the system to be transmitting power. The driving teeth approach the "surface" of the driven teeth, oscillating with less amplitude as time increases. The decrease in oscillation amplitude is most notable in Stage 1. The quantity $S = R_g\theta_g - R_p\theta_p$ waveforms approach the "surfaces" indicated.

From Figure 8, the impacts in both stages increase in magnitude with time and occur at increasingly shorter intervals. The force in Stage 2 is larger because Gear D is being driven by the torque on the input shaft through the gear action of Stage 1. The large inertia of this third rigid body must be overcome solely with the force from Gear C to Gear D in Stage 2. In this way, the Stage 2 impacts carry the energy accumulated in the Stage 1 impacts and have a larger amplitude. The trends in both contact forces observed in Figure 7 continue up to time $\tau = 100$ ms. After 100 ms

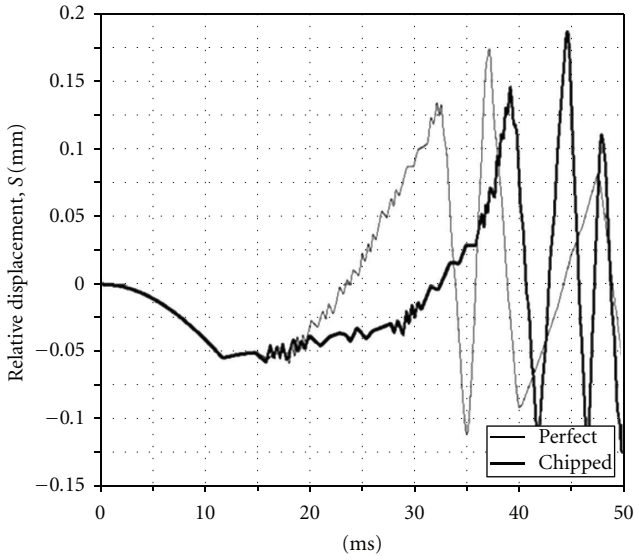

Figure 6: Relative displacement S along the line of action on stage 2 with the initial conditions: input shaft, 167.5 rad/s; intermediate shaft, −73.5 rad/s; output shaft, 12.5 rad/s.

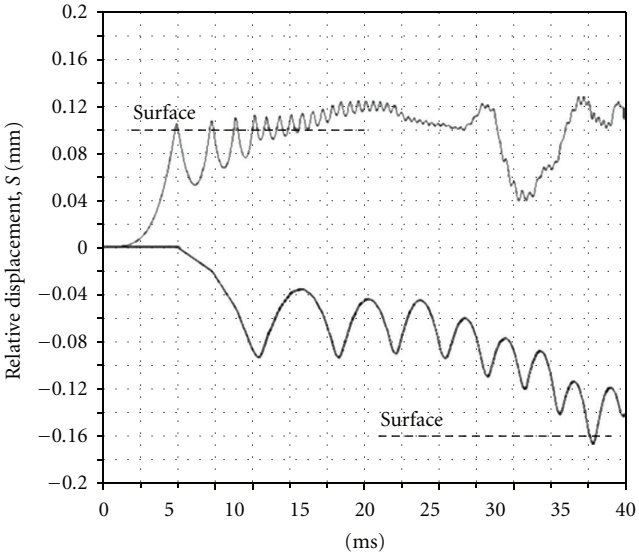

Figure 7: Comparison of relative displacements S along the line of action on Stage 1 and Stage 2 with step input torque 149.123 N-m.

the torque on the input shaft becomes constant, driving the system to steady-state.

In order to demonstrate how the frequency contents of the contact force evolve over time, a joint time-frequency analysis is presented based on the transient start-up conditions. For this procedure, aliasing issues are prevented by using a large number of integration steps and a long simulation duration of 3 seconds. FFT leakage is reduced by overlapping a sliding time sample of 50 ms by 80% and applying a Hamming window to each sample.

From Figure 9(b), the spectral components of the force in Stage 1 follow the exponential form of the applied input

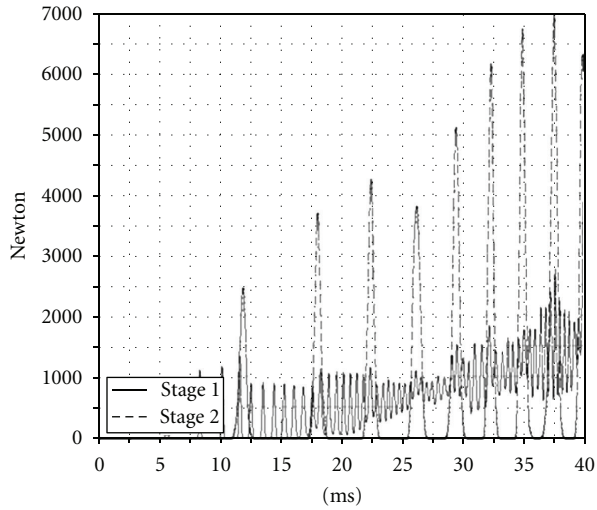

Figure 8: Comparison of the force magnitudes on Stage 1 and Stage 2 with step input torque 149.123 N-m.

torque. The system passes its rated operating speed around 350 ms and continues to accelerate, simulating a start-up condition. The dominant frequencies are the three shaft spin speeds and the two gear mesh frequencies. Because the gear pairs do not share a common factor, only integer multiples of the superharmonics are considered. The largest spectral line is the first gear mesh frequency which begins at $GMF_1 = 1653$ Hz at the first time slice of $t = 600$ ms. The second largest spectral line begins at the first gear mesh superharmonic, $2(GMF_1) = 3306$ Hz. The lines which originate below 100 Hz are the element spin speeds and their respective superharmonics. The largest spin speed amplitude corresponds to input 1X which has a value of 98 Hz at $t = 600$ ms. The exponential step increase is also observed in the magnitudes of each frequency line, something which is not readily available in standard two-dimensional plots. Figure 9(a) shows the trends of the transient magnitude and frequency components of the contact-dynamic force over short time interval.

5. Steady-State Frequency Domain Analysis

To obtain the frequency domain response of Stage 1, a constant angular speed is applied to the input shaft and a small resistive torque on the intermediate and output shafts, shown in Figure 10(a). The value of this resistive torque is one percent of the torque at steady-state operation on each respective shaft. Because the applied torque and the mass moment of inertia of each rigid body are constant, the resistive angular acceleration of each body is also constant. The inclusion of this small torque is critical to obtain acceptable frequency domain results; it dramatically decreases any large variations in force magnitude and emphasizes the repeating patterns in the time domain. Aside from these resistive torques, the system is not loaded and the resulting spectral magnitudes are below 1 kN. The frequency response of Stage 2 is obtained by assigning the output shaft a constant

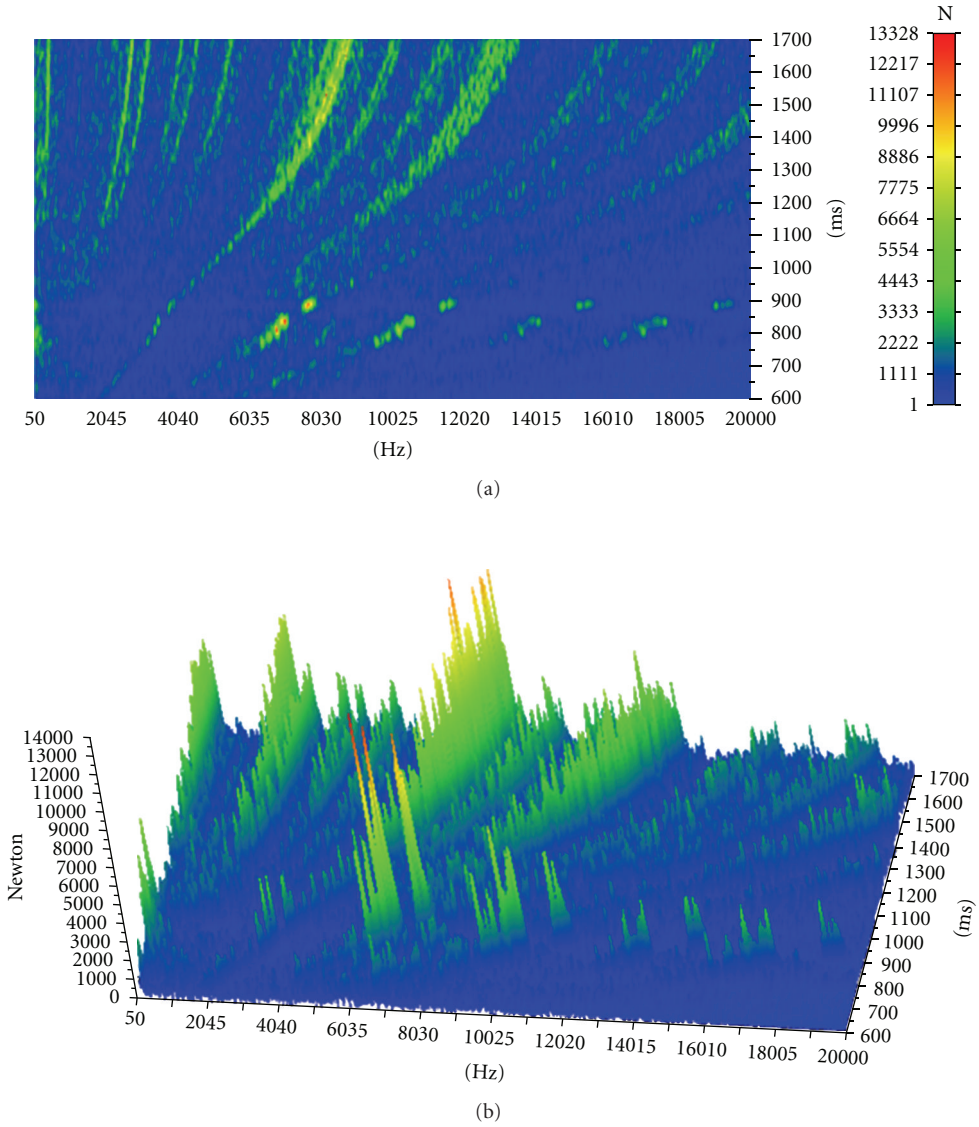

Figure 9: Three-dimensional FFT of force magnitude in Stage 1 for prescribed backlash and perfect geometry with the application of exponential step torque 149.6 N-m.

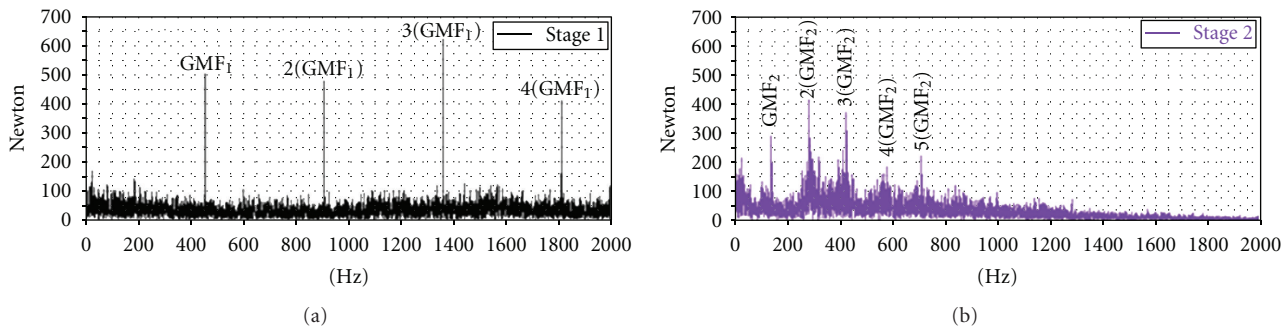

Figure 10: A comparison of frequency domain components of force magnitude on (a) Stage 1 and (b) Stage 2 with prescribed backlash and perfect geometry.

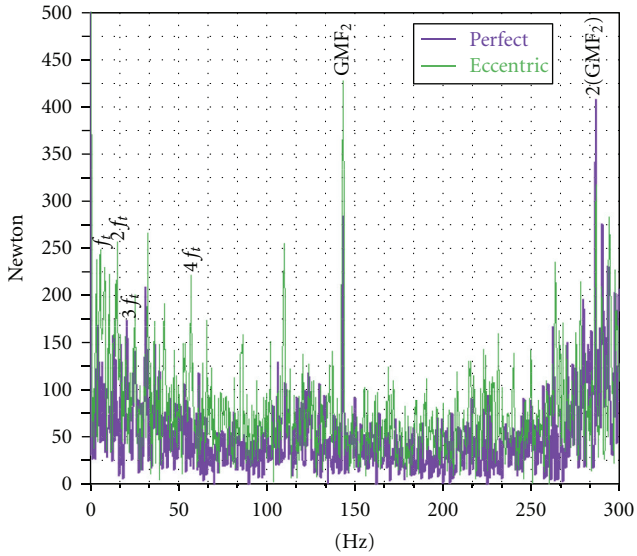

FIGURE 11: Frequency domain components of force magnitude on Stage 2 with an eccentric gear tooth, initial conditions: input shaft, −1.49 N-m, intermediate shaft, −5.27 N-m; output shaft, 12.5 rad/s (1.99 Hz).

angular speed and the input and intermediate shafts a small resistive torque, shown in Figure 10(b). The resistive torques model the rotational friction due to bearings, couplings, and fluid shear in the realistic crank-slider mechanism. An experimental apparatus can maintain the constant speed on the input shaft through an appropriate control system.

The frequency components in each mesh include the respective gear mesh frequencies and their super harmonics. The shaft speeds and hunting tooth frequencies do not appear because the mesh geometry contains prescribed backlash without manufacturing errors. The force magnitudes in Stage 1 are larger because the input pinion has the smallest inertia and experiences the largest angular accelerations for a given impact. If the frequency components under one hundred Newtons are considered erroneous noise, then the first five harmonics of the gear mesh frequency in each stage comprise the vast majority total force vectors.

Stage 1 initial conditions are input shaft, 167.5 rad/s (26.7 Hz); intermediate shaft, −5.27 N-m; output shaft, −20.0 N-m; Stage 2 initial conditions are input shaft, −1.49 N-m, intermediate shaft, −5.27 N-m; output shaft, 12.5 rad/s (1.99 Hz). The contact events in Stage 1 and Stage 2 are coupled together. This is evident in the frequency spectrum as sideband modulation. The force vector in Stage 1 is modulated by the output shaft speed of 1.99 Hz creating relatively small sidebands surrounding the gear mesh harmonics, shown in Figure 10(a). The force vector in Stage 2 is modulated by the input shaft speed of 26.7 Hz, creating the relatively large sideband modulations around the gear mesh harmonics, shown in Figure 10(b).

An eccentric tooth on Gear C results in a significant increase in force magnitude components below the gear mesh frequency, shown in Figure 11. The eccentric tooth comes into mesh once per revolution, causing excitation at the intermediate shaft speed $f_i = 7.6$ Hz and its super harmonics. The influence of this relatively low spin speed excitation decreases as frequency increases; the results of the two spectra are nearly identical after the first superharmonic of the gear meshing frequency. Due to the eccentricity of Gear C, the amplitude of the spectral line at GMF_1 increases 50.4%. This is a potentially new and important vibration signature of the defected gear train.

6. Conclusions

A nonlinear multibody dynamic software model has been developed for a two stage slider-crank mechanism to demonstrate the effects of dynamic loading on gear teeth with defects during transient, start-up, and steady-state operation. The stiffness, force exponent, damping, and friction coefficients for the MSC.IMPACT force algorithm are presented. The dynamic behavior of the intermediate shaft of a two stage slider-crank mechanism is shown to be a superposition of the impact forces acting in each mesh. The geometric error of a chipped tooth on the pinion gear of this mechanism causes a delay in the contact forces in the second stage. A joint time-frequency analysis on a realistic driving step torque reveals spectral components which increase in frequency and magnitude as the crank accelerates through its operating speed. Frequency domain results of steady state operation demonstrate that the response is dominated by the gear mesh frequency and its harmonics.

Acknowledgment

The authors acknowledge the Donald E. Bently Center for Engineering Innovation at California Polytechnic State University San Luis Obispo for support of this work.

References

[1] S. Dubowsky and F. Freudenstein, "Dynamic analysis of mechanical systems with clearances, part 1: formulation of dynamic model," *ASME Journal of Engineering for Industry*, vol. 93, pp. 305–309, 1971.

[2] S. Dubowsky and F. Freudenstein, "Dynamic analysis of mechanical systems with clearances, part 2: dynamic response," *ASME Journal of Engineering for Industry*, vol. 93, pp. 310–316, 1971.

[3] R. C. Azar and F. R. E. Crossley, "Digital simulation of impact phenomenon in sour gear systems," *ASME Journal of Engineering for Industry*, vol. 99, no. 3, pp. 792–798, 1977.

[4] D. C. H. Yang and Z. S. Sun, "A rotary model for spur gear dynamics," *ASME Journal of Mechanisms, Transmissions and Automation in Design*, vol. 107, pp. 529–535, 1985.

[5] H. N. Özgüven and D. R. Houser, "Mathematical models used in gear dynamics—a review," *Journal of Sound and Vibration*, vol. 121, no. 3, pp. 383–411, 1988.

[6] A. Parey and N. Tandon, "Spur gear dynamic models including defects: a review," *Shock and Vibration Digest*, vol. 35, no. 6, pp. 465–478, 2003.

[7] G. Dalpiaz, A. Rivola, and R. Rubini, "Effectiveness and sensitivity of vibration processing techniques for local fault

detection in gears," *Mechanical Systems and Signal Processing*, vol. 14, no. 3, pp. 387–412, 2000.

[8] A. Parey, M. El Badaoui, F. Guillet, and N. Tandon, "Dynamic modelling of spur gear pair and application of empirical mode decomposition-based statistical analysis for early detection of localized tooth defect," *Journal of Sound and Vibration*, vol. 294, no. 3, pp. 547–561, 2006.

[9] S. Ebrahimi and P. Eberhard, "Rigid-elastic modeling of meshing gear wheels in multibody systems," *Multibody System Dynamics*, vol. 16, no. 1, pp. 55–71, 2006.

[10] T. Fakhfakh, F. Chaari, and M. Haddar, "Numerical and experimental analysis of a gear system with teeth defects," *International Journal of Advanced Manufacturing Technology*, vol. 25, no. 5-6, pp. 542–550, 2005.

[11] I. Ciglarič and A. Kidrič, "Computer-aided derivation of the optimal mathematical models to study gear-pair dynamic by using genetic programming," *Structural and Multidisciplinary Optimization*, vol. 32, pp. 153–160, 2006.

[12] M. Pimsarn and K. Kazerounian, "Pseudo-interference stiffness estimation, a highly efficient numerical method for force evaluation in contact problems," *Engineering with Computers*, vol. 19, no. 2-3, pp. 85–91, 2003.

[13] J. Meagher, X. Wu, D. Kong, and C. H. Lee, "A comparison of gear mesh stiffness modeling strategies," in *Proceedings of the IMAC 28th Conference on Structural Dynamics*, Society for Experimental Mechanics, Jacksonville, Fla, USA, February, 2010.

[14] D. Kong, J. Meagher, C. Xu, X. Wu, and Y. Wu, "Nonlinear contact Analysis of gear teeth for malfunction diagnostics," in *Proceedings of the IMAC 26th Conference on Structural Dynamics*, Society for Experimental Mechanics, Orlando, Fla, USA, February, 2008.

[15] MSC Inc., MSC ADAMS reference manual.

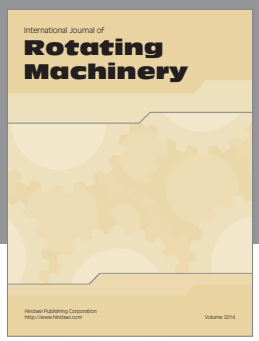

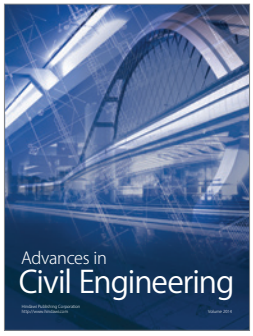

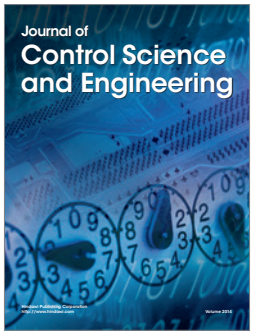

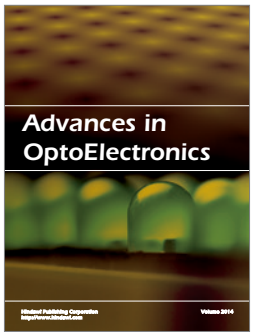

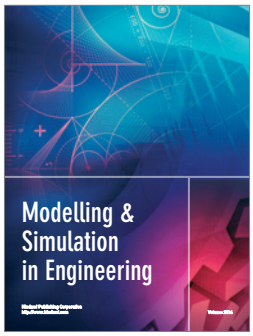

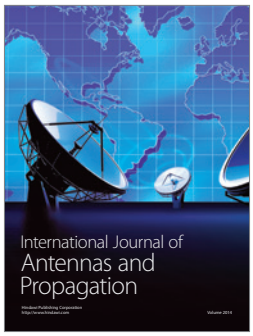

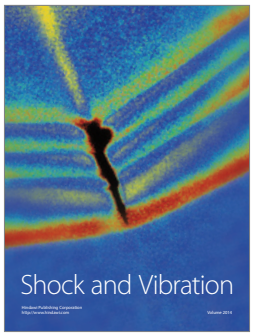

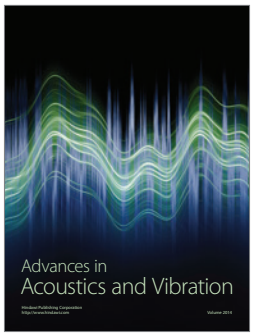

Hindawi

Submit your manuscripts at
http://www.hindawi.com